Materials Chemistry and Physics 136 (2012) 103–111

Contents lists available at SciVerse ScienceDirect

Materials Chemistry and Physics

journal homepage: www.elsevier.com/locate/matchemphys

# Electrochemical behaviour of Al–Zn–Ga and Al–In–Ga alloys in chloride media

D.O. Flamini*, S.B. Saidman

*Instituto de Ingeniería Electroquímica y Corrosión (INIEC), Departamento de Ingeniería Química. Universidad Nacional del Sur, Av. Alem 1253 - 8000 Bahía Blanca - Rep. Argentina*

## HIGHLIGHTS

- Al–Zn–Ga and Al–In–Ga as sacrificial anode.
- Ga does activate Al in ternary alloys.
- Ga homogenous distribution produce Al activation by amalgam formation.
- Al–In–Ga alloy as a more active anode.

## ARTICLE INFO

*Article history:*
Received 19 December 2011
Received in revised form
15 May 2012
Accepted 16 June 2012

*Keywords:*
Aluminium
Sacrificial anode
Al–Zn–Ga alloy
Al–In–Ga alloy
Gallium
Amalgam
Activation mechanism

## ABSTRACT

The influence of Ga content on the electrochemical behaviour of Al–Zn–Ga and Al–In–Ga alloys in chloride acid and acetic acid media was studied. The presence of Ga in concentration greater than 2.5 wt.% causes an open circuit potential (OCP) shifts of Al–Zn–Ga alloys in chloride solution towards more negative values (−1.38 V(SCE)). The OCP for Al–In–Ga alloys in chloride solution varies between −1.62 and −1.73 V(SCE). The anodic behaviour of these ternary alloys can be interpreted in terms of an amalgam mechanism.



## 1. Introduction

Aluminium sacrificial anodes are used to prevent corrosion of iron and steel structures in marine environments. The standard reversible potential of aluminium ($E^{\circ}_{Al^{3+}/Al}$) is −1.90 V(SCE) [1] and it has a high capacity (2980 Ah kg$^{-1}$). However, pure aluminium and its alloys exposed to the air rapidly form a layer of protective oxide. Breakdown of the protective oxide results in seawater pitting attack at a potential of −0.80 V(SCE) [2] and this causes a decrease of anode efficiency.

Aluminium as an anodic material is of interest both in cathodic protection system and in energy storage systems, like primary batteries [3], fuel cells [4,5] and in secondary batteries that utilise non-aqueous electrolytes [6].

The addition of alloying elements such as Hg, In, Ga, Bi, Zn or Sn changes the pitting potential of aluminium towards more electronegative values in the presence of chloride ions [7–9]. Some alloying elements (Hg, Ga and In) result in more uniform dissolution in solutions containing aggressive ions. However, the toxicity of Hg means that other low melting point elements such as In and Ga are more acceptable additions.

Several studies on the activation of Al–In [8], Al–Ga [10–16] and Al–Zn [8,17] alloys have been carried out and various different mechanisms have been proposed to explain the activation effect of these elements. Alloys such as Al–Zn–Hg [18], Al–Zn–Sn [19], Al–Zn–In [20–23] and Al–Zn–Ga [10] have received particular attention due to the operating potential and their high current efficiency associated with a lower hydrogen evolution reaction.

Aluminium activation by Ga has been related to the increased adsorption of chloride ion at more negative potentials [13,14]. Tuck et al. have proposed that Ga particles at the metal/oxide interface of Al–Ga alloy cause local thinning of the oxide film [11]. In previous work we have proposed an amalgam-activation mechanism where a minimum amount of liquid Ga in true metallic contact with Al is needed for surface activation [24]. Liquid Ga diffusion on an Al surface undermines and detaches the oxide, increasing the active area. An active potential (−1.50 V(SCE)) was reported at the

* Corresponding author. Tel./fax: +54 291 4595182.
*E-mail address:* dflamini@uns.edu.ar (D.O. Flamini).

0254-0584/$ – see front matter © 2012 Elsevier B.V. All rights reserved.
http://dx.doi.org/10.1016/j.matchemphys.2012.06.036

amalgam/solution interface. The presence of Zn as alloying component in the Al–Zn–Ga alloy helps the development of a critical surface concentration of Ga to produce the amalgam [25].

In the present study the electrochemical behaviour of Al–Zn–Ga and Al–In–Ga ternary alloy has been analysed by considering the influence of Ga concentration onto the activation mechanism using potentiodynamic, open circuit potential (OCP) versus time and Tafel measurements. Surface characterisation was carried out using scanning electron microscopy (SEM) and quantitative energy dispersive X-ray analyser.

## 2. Material and methods

The ternary Al–Zn–Ga and Al–In–Ga alloys were prepared with nominal compositions of Al–4.0 wt.%Zn–*x*wt.%Ga ($x = 0.5$, 2.5 and 5.0) and Al–0.2 wt.%In–*y* wt.%Ga ($y = 0.5$, 2.5 and 5.0), from pure Al, Zn, Ga and In (Aldrich Chemical Co.), which were etched in 2% nitric acid in ethanol and then placed into a cylindrical graphite crucible. The samples were melted above 660 °C under an inert atmosphere of Ar gas and then were stirred until reach a homogeneous mixture of elements. After that, the crucible was then quenched into water at room temperature to maintain a homogeneously distribution of alloying components in solid solution. The Zn and In contents correspond to those of the most important commercial Al alloys used as sacrificial anodes.

After chemical etching, the microstructure of Al ternary alloys was characterised with scanning electron microscopy (SEM) and the elemental composition was estimated with a quantitative energy dispersive X-ray analyser. The Al–4.0 wt.%Zn–5.0 wt.%Ga alloy was etched with Keller reagent (1 ml HF, 1.5 ml HCl, 2.5 ml $HNO_3$ and 95 ml $H_2O$). Due to the higher reactivity observed for the Al–0.2 wt.%In–5.0 wt.%Ga alloy, its microstructure was revealed by chemical etching with diluted fluoride acid (1 % (v/v)) solution.

Samples of the cast alloys embedded in a Teflon holder with an exposed area of 0.070 $cm^2$ were used as the working electrodes. The exposed surface area was abraded with 1000 grade emery paper followed by 1 μm grit alumina suspensions, then degreased with acetone and rinsed with triply distilled water. The electrode was then immediately transferred to a three electrode compartment electrochemical cell (250 mL). All potentials were measured against a saturated calomel electrode (SCE) connected through a Luggin–Haber capillary tip and a Pt sheet was used as the counter-electrode.

Electrochemical measurements were carried out by means a potentiostat-galvanostat PAR Model 273A using a SoftCorr™ II software. A dual stage ISI DS 130 SEM and an EDAX 9600 quantitative energy dispersive X-ray analyser were used to examine the electrode surface characteristics.

Linear anodic polarisation curves in acid chloride solution were recorded at a scan rate of 0.001 V $s^{-1}$ from −1.80 V(SCE) until a current density value of 30 mA $cm^{-2}$ was reached. The anodic polarisation curves in acetic acid solution were registered at the same scan rate in the potential range between −1.80 and −0.70 V(SCE).

Tafel plots were used to determine the electrochemical parameters (anodic Tafel slope ($\beta_a$), cathodic Tafel slope ($\beta_c$), corrosion potential ($E_{corr}$) and corrosion current density ($i_{corr}$)). The $i_{corr}$ was obtained by extrapolation, to $E_{corr}$, from the linear part of anodic and/or cathodic branches of the Tafel plots.

The test solutions (0.5 M NaCl and 0.5 M HAc) were prepared from analytical grade chemicals and triple-distilled water. The pH of the chloride solution was adjusted with HCl to 3. Measurements were made under a purified nitrogen gas saturated atmosphere at 25 °C. Each experiment was repeated three times to ensure reproducibility with variations below ±5%.

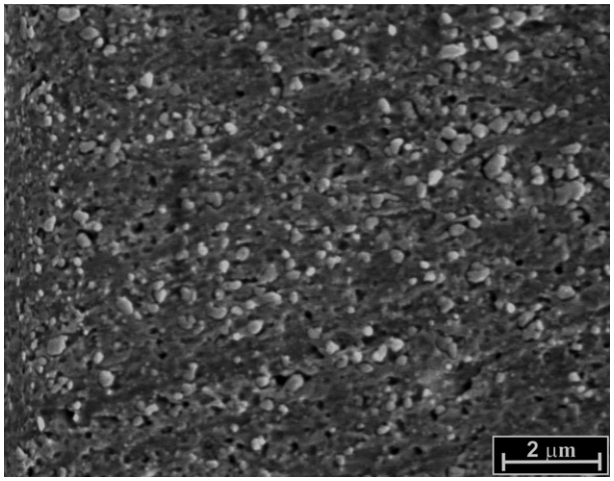


**Fig. 1.** Microstructure of the Al–4.0 wt.%Zn–5.0 wt.%Ga revealed after chemical etching with Keller reagent for 60 s.

## 3. Results

### 3.1. Microstructure characterisation of ternary alloys

EDX analysis of the abraded Al–Zn–Ga alloy showed the presence of the following elements: 2.10 wt.% Zn, 5.08 wt.% Ga and rest Al. After chemical etching with Keller reagent for 60 s, the Al–4.0 wt.%Zn–5.0 wt.%Ga alloy presents a chill structure consisting of small equiaxed (equal-sized) crystals homogeneously distributed and randomly orientated in the matrix phase (Fig. 1). It was observed that an increment in the etching time produces a smoother matrix surface with a more number of small crystals (0.5 μm in diameter) but with an increase in spherical holes as a result of chemical dissolution. EDX analysis performed in different small crystals always showed an increasing contain of Ga (6.32 wt.%) in comparison with the matrix phase (4.38 wt.%). The presence of Zn was not detected due to its preferential dissolution.

In the case of Al–4.0 wt.%Zn–0.5 wt.%Ga and Al–4.0 wt.% Zn–2.5 wt.%Ga alloys, the revealed microstructure was similar to that obtained for the alloy with more concentration of Ga (5.0 wt.%), although with a less amount of small crystals (0.5 μm in diameter) enriched in Ga content with respect to the matrix phase.

The chemical etching of the Al–0.2 wt.%In–5.0 wt.%Ga alloy with diluted fluoride acid solution for 15 s, also revealed a chill structure although a greater density of small crystals in comparison with the

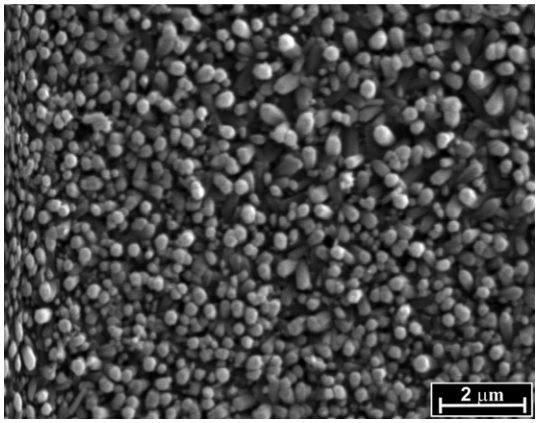


**Fig. 2.** Microstructure of the Al–0.2 wt.%In–5.0 wt.%Ga revealed after chemical etching with diluted fluoride acid (1 % (v/v) HF) aqueous solution for 15 s.

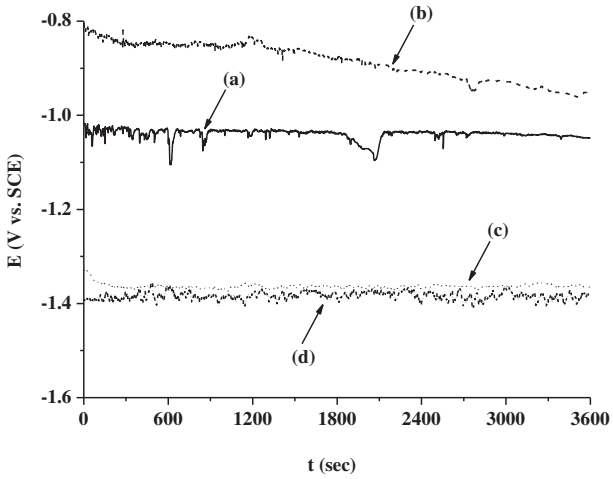


**Fig. 3.** Open circuit potential (OCP) vs. time in 0.5 M NaCl, pH 3 solution: (a) Al–4.0 wt.%Zn, (b) Al–4.0 wt%Zn–0.5 wt.%Ga, (c) Al–4.0 wt.%Zn–2.5 wt.%Ga and (d) Al–4.0 wt.%Zn–5.0 wt.%Ga.

Al–4.0 wt.%Zn–5.0 wt.%Ga alloy was observed (Fig. 2). The crystals had a microtube appearance and they were preferential oriented. The number of these crystals decreased as the Ga content diminished. EDX analysis of the Al–0.2 wt.%In–5.0 wt.%Ga alloy surface after chemical etching showed the presence of the following components: 6.02 wt. % Ga, 7.70 wt.% O and rest Al. The presence of In was not detected before and after chemical etched by EDX analyser due to its weight percentage is lower than the detection limit.

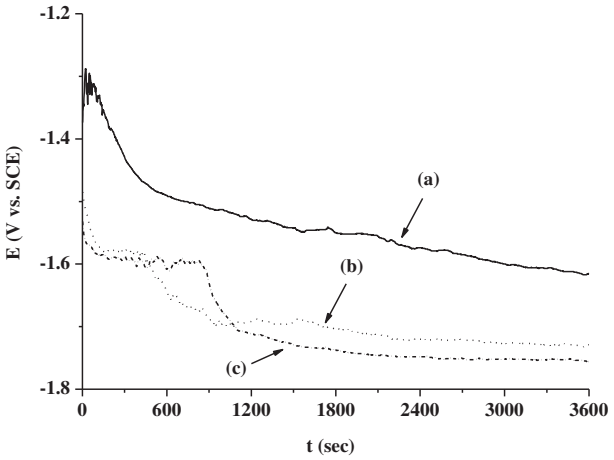


**Fig. 5.** Open circuit potential (OCP) vs. time in 0.5 M NaCl, pH 3 solution: (a) Al–0.2 wt.%In–0.5 wt.%Ga, (b) Al–0.2 wt.%In–2.5 wt.%Ga and (c) Al–0.2 wt.% In–5.0 wt.%Ga.

### 3.2. Studies in the acidified sodium chloride solution

#### 3.2.1. Open circuit potential (OCP) – time measurements

The activation process can be studied by analysing the open circuit potential (OCP) against time for the different ternary alloys. The OCP value for Al–4.0 wt.%Zn alloy (Fig. 3, curve a) was more negative than the OCP value measured for Al–4.0 wt.%Zn–0.5 wt.% Ga alloy (Fig. 3, curve b). It is possible that the Ga present in the ternary alloy is oxidised to $Ga_2O_3$ imparting some sort of passivity.

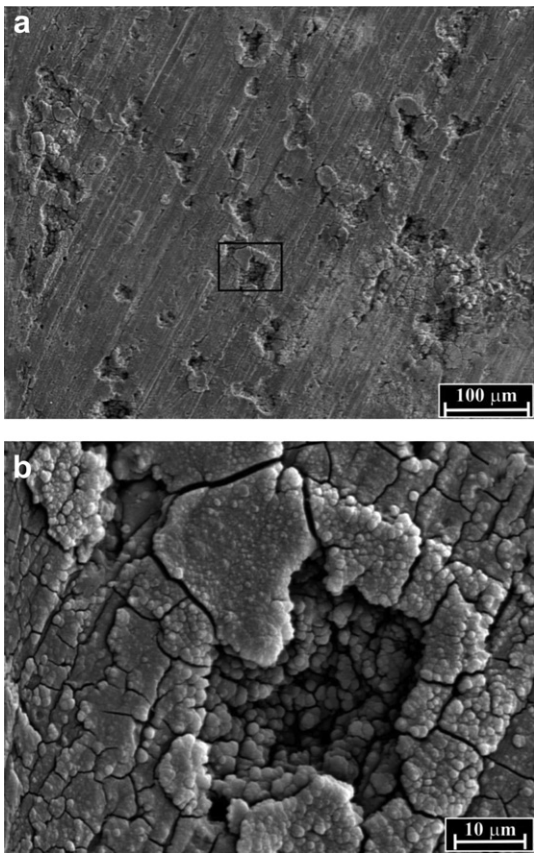


**Fig. 4.** (a) SEM micrograph of attacked areas onto Al–4.0 wt.%Zn–5.0 wt.%Ga alloy surface obtained after OCP measurement during 3600 s in 0.5 M NaCl, pH 3 solution; and (b) magnified SEM image of the attacked area.

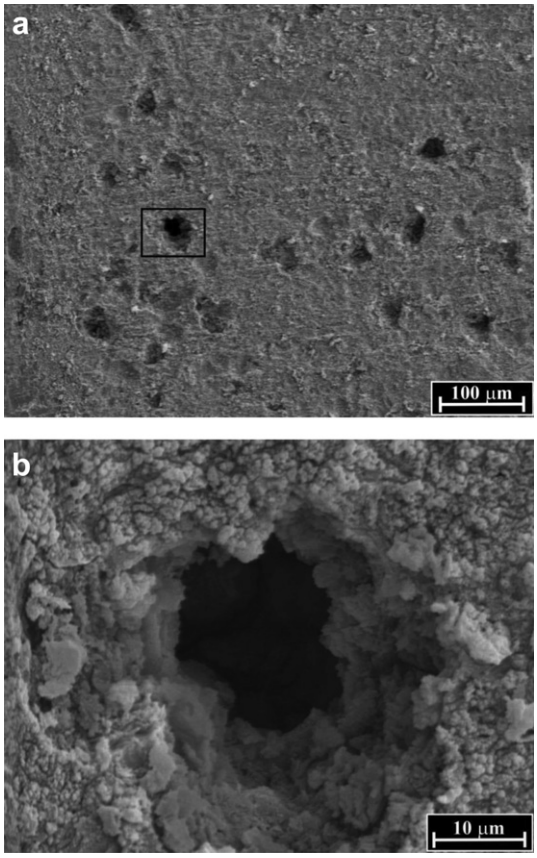


**Fig. 6.** (a) SEM micrograph of attacked areas onto Al–0.2 wt.%In–5.0 wt.%Ga alloy surface obtained after OCP measurements during 3600 s in 0.5 M NaCl, pH 3 solution; and (b) magnified SEM image of the attacked area.

A similar result was obtained by Aragon et al. [10] who found that additions of Zn to Al–Ga alloys containing 0.2 or 0.5 wt.% of Ga produced a positive shift in the free potential compared with the binary Al–Ga alloys. The OCP values of the higher gallium Al–Zn–Ga alloys were shifted in the negative direction (Fig. 3). For Al–4.0 wt.%Zn–2.5 wt.%Ga and Al–4.0 wt.%Zn–5.0 wt.%Ga alloys the OCP reached a constant value of −1.36 and −1.38 V(SCE) (Fig. 3, curves c and d), respectively. The higher amplitude of the potential spikes observed for Al–4.0 wt.%Zn–5.0 wt.%Ga alloys suggests a more active condition.

After OCP measurements, the SEM micrograph of the Al–4.0 wt.%Zn–5.0 wt.%Ga alloy in Fig. 4a shows attacked areas distributed homogenously over the surface. The higher magnification image of the attacked area (Fig. 4b) shows a mud-cracked film of corrosion products.

For the case of Al–In–Ga alloys the OCP value decays to values of −1.62, −1.73 and −1.76 V(SCE) for Al–0.2 wt.%In–0.5 wt.%Ga, Al–0.2 wt.%In–2.5 wt.%Ga and Al–0.2 wt.%In–5.0 wt.%Ga, respectively (Fig. 5). Thus, the OCP was displaced to more negative potentials as the Ga content increased. The more negative value of the OCP indicates a more active state compared to the Al–Zn–Ga alloys.

The active state of the ternary Al–4.0 wt.%Zn–5.0 wt.%Ga and Al–0.2 wt.%In–5.0 wt.%Ga alloys was maintained for longer immersion times (7 days). On the other hand, the pH of chloride solution practically did not change during this period.

Pits as well as general corrosion appear onto the Al–0.2 wt.% In–5.0 wt.%Ga alloy surface after OCP measurement (Fig. 6a). The higher magnification SEM image (Fig. 6b) shows a deep cavity surrounded by corrosion products.

Hydrogen evolution *was observed* for both Al–Zn–Ga and Al–In–Ga alloys, but the rate of evolution was higher for the Al–In–Ga alloys compared to the Al–Zn–Ga alloys with the same Ga content. The volume of hydrogen produced after 24 h at OCP conditions was measured with a eudiometer. The volume collected was 0.4 mL for Al–4.0 wt.%Zn–5.0 wt.%Ga alloy and 8.6 mL for Al–0.2 wt.%In–5.0 wt.%Ga alloy, respectively.

OCP measurements were also performed in acidified chloride for a liquid Ga–4.0 wt.%In amalgam and also for an In electrode with a Ga particle (50 mg) mechanically attached. In both cases the OCP was coincident with those of the pure metals, Ga and In, respectively [26,27]. This suggested that there is no formation of an intermetallic compound between In and Ga that modified the OCP value of the pure metals.

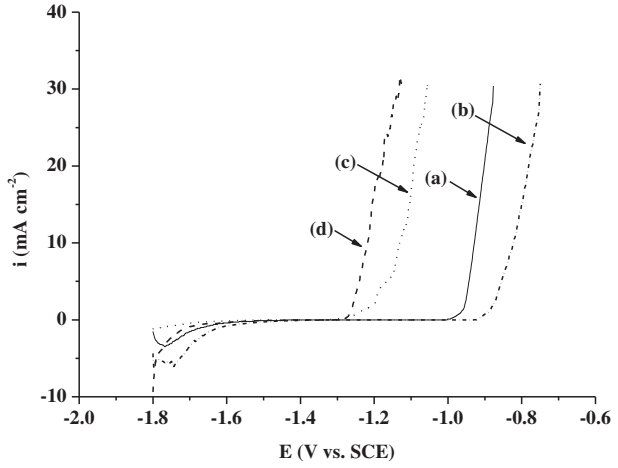


**Fig. 7.** Linear polarisation curve registered at 0.001 V s$^{-1}$ in a 0.5 M NaCl, pH 3 solution for: (a) Al–4.0 wt.%Zn, (b) Al–4.0 wt.%Zn–0.5 wt.%Ga, (c) Al–4.0 wt.%Zn–2.5 wt.%Ga and (d) Al–4.0 wt.%Zn–5.0 wt.%Ga.

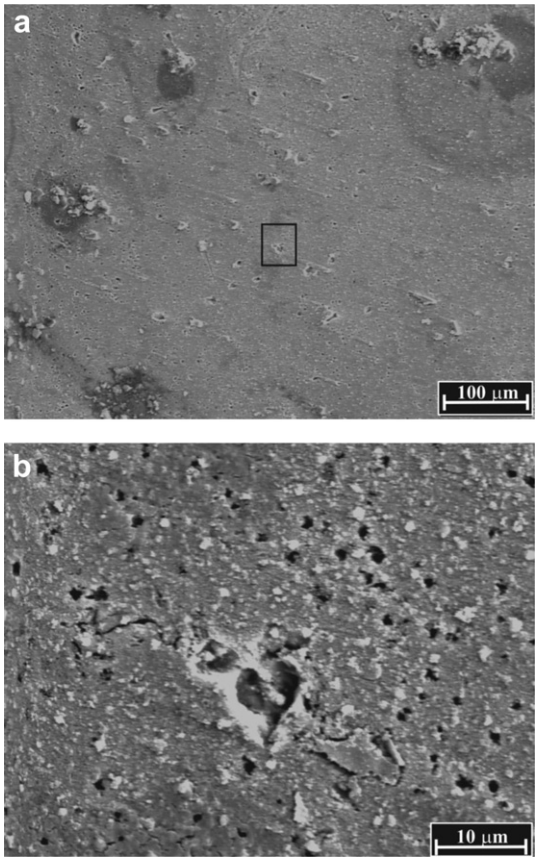


**Fig. 8.** (a) SEM micrograph of attacked areas onto Al–4.0 wt.%Zn–5.0 wt.%Ga alloy surface after linear anodic polarisation in a 0.5 M NaCl, pH 3 solution, and (b) magnified SEM image of the attacked area.

### 3.2.2. Polarisation measurements

The influence of Ga content in the Al–Zn–Ga ternary alloy was analysed by linear anodic polarisation (Fig. 7). The onset of active dissolution for Al–4.0 wt.%Zn–0.5 wt.%Ga alloy was produced at a more positive potential than for the Al–4.0 wt.%Zn alloy (Fig. 7, curves a and b). When the Ga content of the Al–Zn–Ga ternary alloy was greater than 2.5 wt.%, the beginning of active behaviour was produced at more negative potential (c.a. −1.30 V(SCE)) (Fig. 7, curves c and d) with a considerable reduction of the passive region. According to Frumkin et al. [28] the potential of zero charge ($E_{pzc}$) measured for Ga in 1.0 M KCl solution was −1.10 V(SCE). This means that $Cl^-$ ion adsorption onto Al–Zn–Ga surface will be produced when the $E_{pzc}$ of Ga is overcome, that is, when the potential is more positive than −1.10 V(SCE). Thus, the onset of the depolarised pitting process of Al–4.0 wt.%Zn–*x* wt.%Ga ($x = 2.5$ and 5.0) alloy near to −1.30 V(SCE) could be associated with the amalgam activation mechanism, as was proposed in a previous paper [25].

Fig. 8 shows a SEM image of the Al–4.0 wt.%Zn–5.0 wt.%Ga alloy surface after a linear anodic polarisation to a current density value of 10 mA cm$^{-2}$. Irregular pits were uniformly distributed onto the electrode surface (Fig. 8a), in agreement with previous results obtained for Al–5.6 wt%Zn–3.0 wt.%Ga ternary alloys [25]. A magnified image of the attacked area (Fig. 8b) shows that the attack started in the enriched Ga zone of the alloy (small crystal observed in Fig. 1).

Fig. 9 shows the potentiodynamic anodic polarisation for Al–In–Ga alloy at 0.001 V s$^{-1}$ in 0.5 M NaCl, pH 3 solution. The active state of Al–In–Ga alloys initiates at more electronegative potentials compared to the Al–Zn–Ga alloys. The dissolution

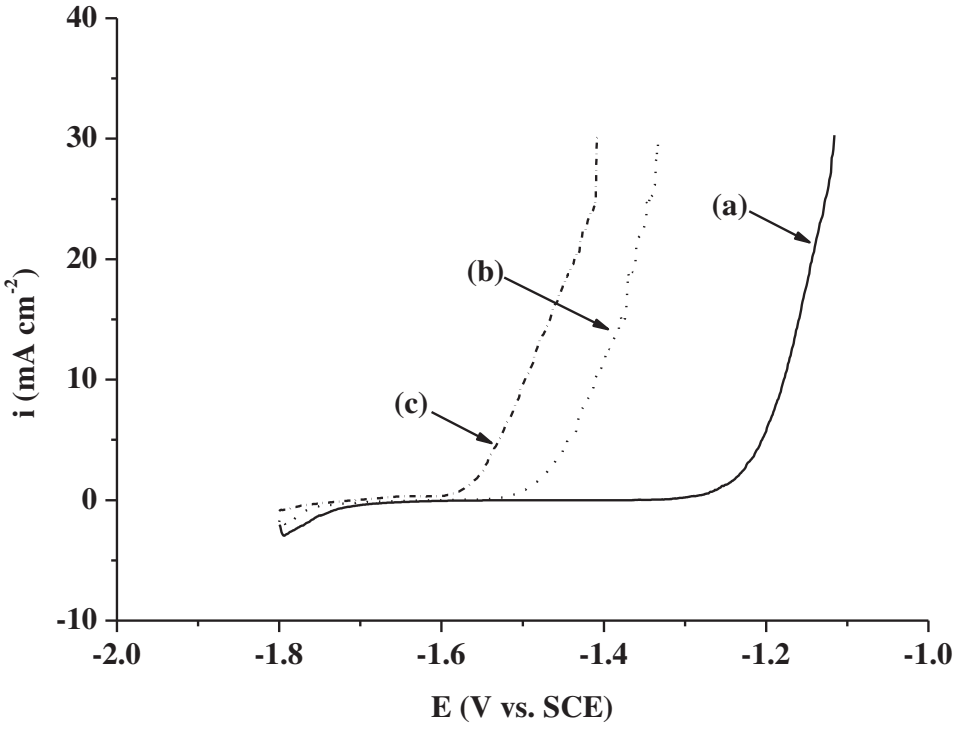


**Fig. 9.** Linear polarisation curve registered at 0.001 V $s^{-1}$ in a 0.5 M NaCl, pH 3 solution for: (a) Al–0.2 wt.%In–0.5 wt.%Ga, (b) Al–0.2 wt.%In–2.5 wt.%Ga and (c) Al–0.2 wt.% In–5.0 wt.%Ga.

process of Al–In–Ga starts at −1.25, −1.50 and −1.60 V(SCE) for 0.5, 2.5 and 5.0 wt.% of Ga content, respectively. The presence of both In and Ga as alloying elements in the Al matrix produces a reduction of the passive region. A similar activation processes was obtained previously with Ga–Al amalgam electrodes [26].

Fig. 10 shows a SEM image of the Al–0.2 wt.%In–5.0 wt.%Ga alloy surface after a linear anodic polarisation to a current density value of 10 mA $cm^{-2}$. A more attacked surface was observed for Al–In–Ga alloys compared to Al–Zn–Ga alloys (Fig. 10a vs. Fig. 8a). Deep cavities (Fig. 6b) were found on the Al–In–Ga alloy surface.

Tafel plots were obtained after OCP stabilisation (3600 s) starting from −0.20 V(SCE) to 0.20 V(SCE) vs. OCP and the potential scan rate was 0.001 V $s^{-1}$. For Al–4.0 wt.%Zn and Al–4.0 wt.% Zn–0.5 wt.%Ga alloys, the $i_{corr}$ values were estimated by Tafel extrapolation of anodic and cathodic Tafel lines to the $E_{corr}$ (Fig. 11, curves a and b). For an accurate extrapolation, at least one of the branches of the polarisation curve should exhibit Tafel behaviour. The $i_{corr}$ values of Al–4.0 wt.%Zn–$x$ wt.%Ga ($x = 2.5$ and 5.0) alloys were estimated by extrapolation of the anodic Tafel lines back to the corresponding values of $E_{corr}$ (Fig. 11, curves c and d). In both cases, the anodic branch showed a considerable increase in current density for a small increase in potential indicating that active depolarised alloy dissolution was occurred. The anodic Tafel slope ($\beta_a$) decreases with Ga content (Table 1). Moreover, the presence of a mud-cracked film of corrosion products formed after OCP stabilisation (3600 s) hinders the cathodic reduction reaction. Thus, the cathodic limiting current can be attributed to the diffusion of proton ions in the corrosion products layer (Fig. 11, curves c and d).

An appreciable displacement of $E_{corr}$ in the negative direction and a higher $i_{corr}$ value were observed for Al–Zn–Ga alloys, only when the Ga content was between 2.5 and 5.0 wt.% (Fig. 11 and Table 1). For Al–0.2 wt.%In–0.5 wt.%Ga alloy, the $i_{corr}$ value was also estimated by Tafel extrapolation of anodic and cathodic Tafel lines to the $E_{corr}$ (Fig. 12, curve a). Nevertheless, the $i_{corr}$ values of

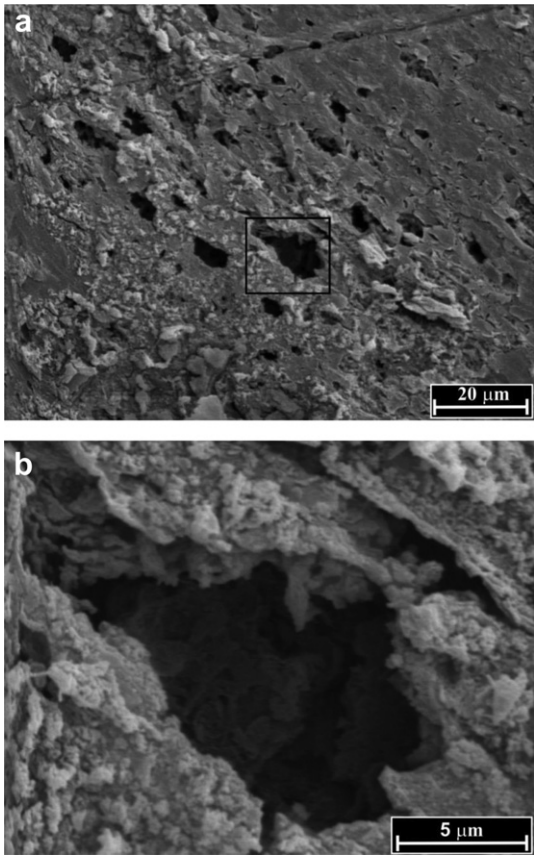


**Fig. 10.** (a) SEM micrograph of attacked areas onto electrode surface of Al–0.2 wt.% In–5.0 wt.%Ga alloy after linear anodic polarisation in a 0.5 M NaCl, pH 3 solution, and (b) magnified SEM image of the attacked area.

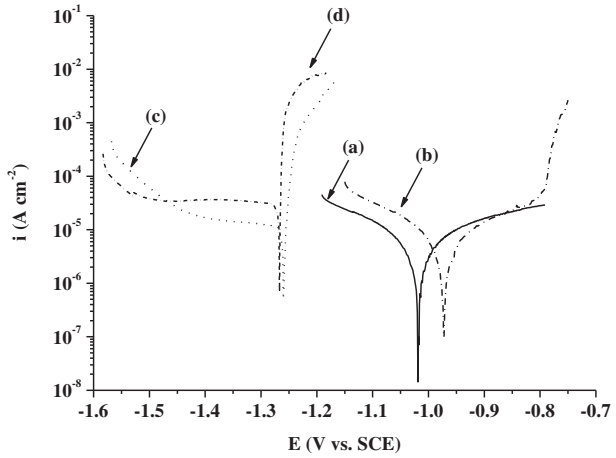


**Fig. 11.** Tafel curves registered after OCP measurements during 3600 s in 0.5 M NaCl, pH 3 solution at 0.001 V s$^{-1}$ for: (a) Al–4.0 wt.%Zn, (b) Al–4.0 wt.%Zn–0.5 wt.%Ga, (c) Al–4.0 wt.%Zn–2.5 wt.%Ga and (d) Al–4.0 wt.%Zn–5.0 wt.%Ga.

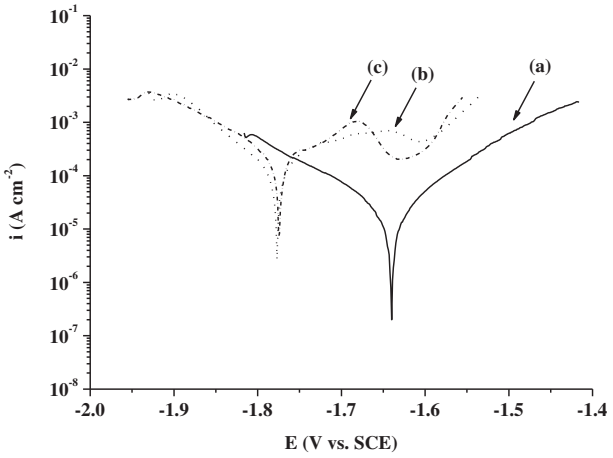


**Fig. 12.** Tafel curves registered after OCP measurements during 3600 s in 0.5 M NaCl, pH 3 solution at 0.001 V s$^{-1}$ for: (a) Al–0.2 wt.%In–0.5 wt.%Ga, (b) Al–0.2 wt.% In–2.5 wt.%Ga and (c) Al–0.2 wt.%In–5.0 wt.%Ga.

Al–0.2 wt.%In–*y* wt.%Ga ($y = 2.5$ and 5.0) alloys were estimated by extrapolation of the cathodic Tafel lines back to the corresponding values of $E_{corr.}$ In both cases, the anodic branch did not present Tafel behaviour (Fig. 12, curves b and c).

The displacement of $E_{corr}$ values was more evident in the Tafel plots for the Al–In–Ga alloys (Fig. 12), where less Ga content is required (>0.5 wt.%) to reach the active state in comparison to Al–Zn–Ga alloys. The electrochemical parameters for Al–In–Ga alloys in chloride acid media are summarised in Table 1, showing that an increase in the Ga content produces more negative $E_{corr}$ and higher $i_{corr}$ values.

### 3.3. Studies in acetic acid solution

#### 3.3.1. Open circuit potential (OCP) – time measurements

In order to analyse the influence of a non-aggressive anion on the activation process of Al–Zn–Ga and Al–In–Ga alloys, the OCP of these ternary alloys was measured in 0.5 M HAc, pH 3 solution.

The OCP value of the Al–Zn–Ga alloy depended on the Ga content. The OCP value for Al–4.0 wt.%Zn alloy (Fig. 13, curve a) was more negative than the OCP value measured for Al–4.0 wt.% Zn–0.5 wt.%Ga alloy (Fig. 13, curve b). As the Ga concentration increased, the OCP value was shifted to more negative potentials. The Al–4.0 wt.%Zn–5.0 wt.%Ga alloy reaches an OCP value of −1.05 V(SCE) in acetic acid solution (Fig. 13, curve d), which is less active in comparison to that obtained in chloride acid media (Fig. 7, curve d). This potential value was previously measured using a Ga–Al saturated amalgam formed on Al surface with Ga mechanically attached [29].

The SEM micrograph of the Al–4.0 wt.%Zn–5.0 wt.%Ga alloy after OCP measurements in acetic acid media showed an attacked area surrounded by corrosion products distributed homogenously over all surface (Fig. 14a). The higher magnification SEM image of the attacked area (Fig. 14b) shows the mud-cracked corrosion product consisted of aluminium oxide/hydroxide inside and outside the cavity. The presence of the corrosion product film formed on the Al–Zn–Ga alloy surface in acetic acid media could be responsible for the lower activation potential as has previously been suggested for Al–Zn alloy in the presence of $In^{3+}$ [30].

Very active OCP values were measured for Al–0.2 wt.%In–*y*wt.% Ga ($y = 0.5$, 2.5 and 5.0) alloys even in acetic acid media (Fig. 15). A similar OCP value was previously reported for Ga mechanically attached to the Al surface in contact with HAc solution at 50 °C [26]. This very negative potential was associated with a physical corrosion process (amalgamation) followed by an electrochemical corrosion reaction with vigorous hydrogen evolution at the amalgam/solution interface.

A smoother surface was observed for the Al–In–Ga alloys compared to the Al–Zn–Ga alloys after OCP measurements in acetic acid media (Fig. 16 and Fig. 14). The presence of liquid Ga on the Al surface facilitates the Ga–Al amalgam formation by mean of a wetting action to produce this type of attack morphology.

**Table 1**
Electrochemical parameters obtained from Tafel plots Al–Zn, Al–Zn–Ga and Al–In–Ga alloys in 0.5 M NaCl, pH 3 solution.

| Electrode material | $E_{corr}$ (V(SCE)) | $\beta_a$ (mV dec$^{-1}$) | $\lvert\beta_c\rvert$ (mV dec$^{-1}$) | $i_{corr}$ (μA cm$^{-2}$) |
|---|---|---|---|---|
| Al–4.0 wt.%Zn | −1.02 | 311 | 219 | 6 |
| Al–4.0 wt.%Zn–0.5 wt.%Ga | −0.97 | 227 | 180 | 7 |
| Al–4.0 wt.%Zn–2.5 wt.%Ga | −1.26 | 17 | – | 11 |
| Al–4.0 wt.%Zn–5.0 wt.%Ga | −1.27 | 11 | – | 38 |
| Al–0.2 wt.%In–0.5 wt.%Ga | −1.64 | 105 | 126 | 25 |
| Al–0.2 wt.%In–2.5 wt.%Ga | −1.78 | – | 74 | 95 |
| Al–0.2 wt.%In–5.0 wt.%Ga | −1.78 | – | 120 | 236 |

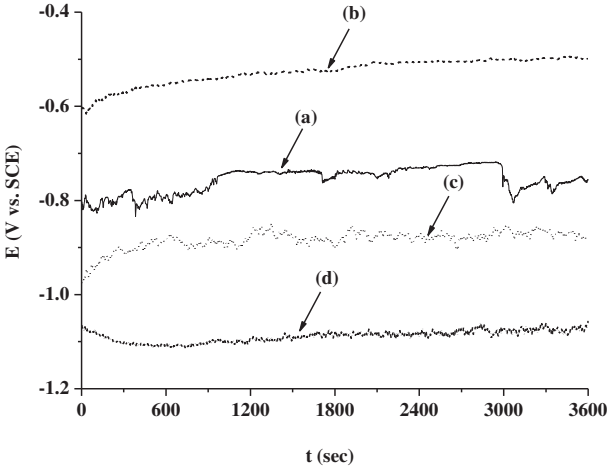


**Fig. 13.** Open circuit potential (OCP) vs. time in 0.5 M HAc, pH 3 solution: (a) Al–4.0 wt% Zn, (b) Al–4.0 wt%Zn–0.5 wt.%Ga, (c) Al–4.0 wt.%Zn–2.5 wt.%Ga and (d) Al–4.0 wt.% Zn–5.0 wt.%Ga.

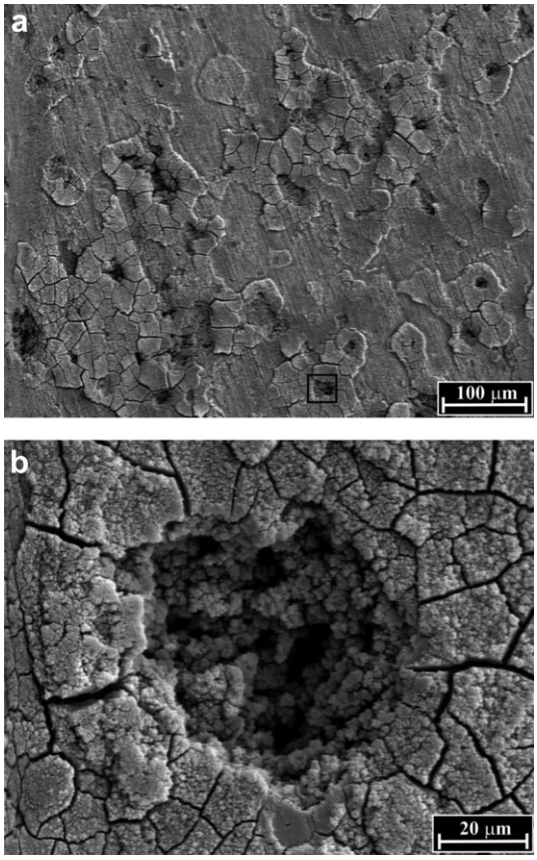


**Fig. 14.** (a) SEM micrograph of attacked areas onto Al–4.0 wt.%Zn–5.0 wt.%Ga alloy surface obtained after OCP measurement during 3600 s in 0.5 M HAc, pH 3 solution; and (b) magnified SEM image of the attacked area.

### 3.3.2. Polarisation measurements

Potentiodynamic anodic polarisation was also performed in acetic acid media for the Al–Zn, Al–Zn–Ga and Al–In–Ga alloys (Figs. 17 and 18, respectively). Anodic dissolution of the Al–4.0 wt% Zn alloy started at −0.80 V(SCE) (Fig. 17, curve a). No electrodissolution process takes place for Al–4 wt.%Zn–0.5 wt.%Ga in the potential range analysed (Fig. 17, curve b). An active dissolution of the Al–Zn–Ga alloys were produced at −0.92 V(SCE) (Fig. 17, curve c) and −1.00 V(SCE) (Fig. 17, curve d) for a Ga content of 2.5 and 5.0 wt.%, respectively. An increase in the anodic slope for the Al–Zn–Ga alloy was observed as a consequence of higher Ga content (Fig. 17).

Fig. 18 shows the linear anodic polarisation for the Al–In–Ga alloys containing different amounts of Ga. A linear current increase was observed and much higher currents were measured for the higher Ga content. On the other hand, the onset of anodic current increase was shifted to more negative potential in concordance with the OCP displacement.

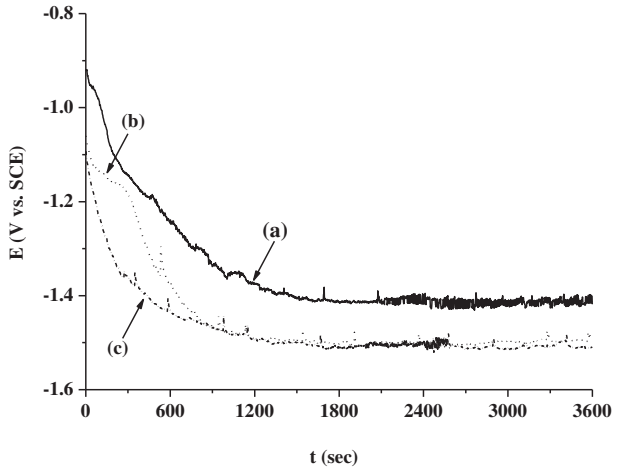


**Fig. 15.** Open circuit potential (OCP) vs. time in 0.5 M HAc, pH 3 solution: (a) Al–0.2 wt.%In–0.5 wt.%Ga, (b) Al–0.2 wt.%In–2.5 wt.%Ga and (c) Al–0.2 wt.% In–5.0 wt.%Ga.

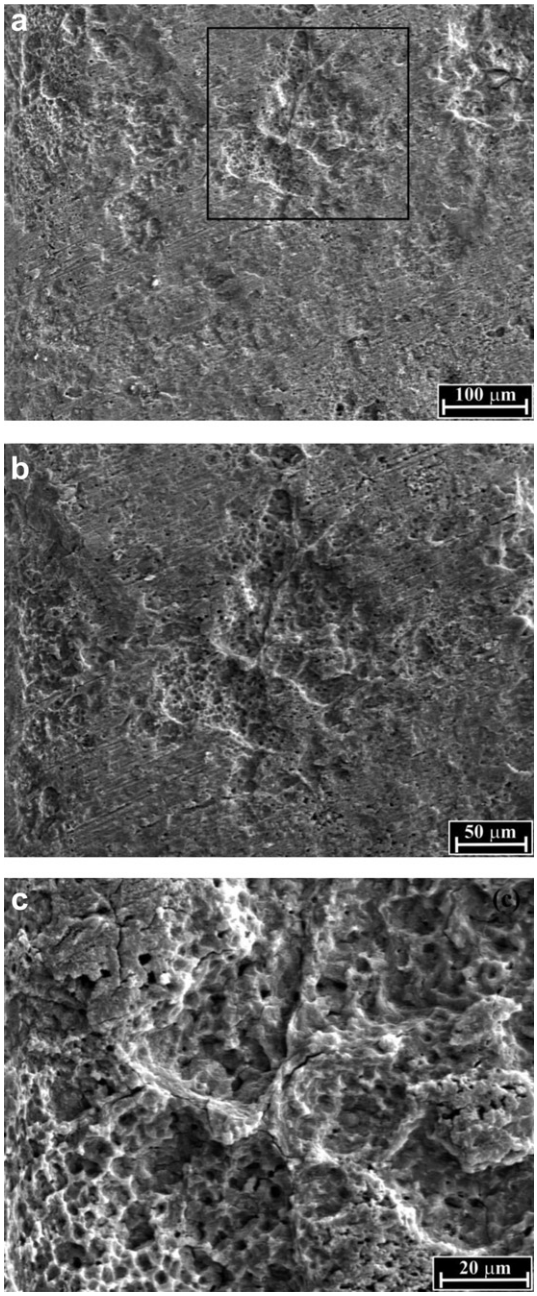


**Fig. 16.** (a) SEM micrograph of attacked areas onto Al–0.2 wt.%In–5.0 wt.%Ga alloy surface after OCP measurement during 3600 s in 0.5 M HAc, pH 3 solution; (b) magnified SEM image of the attacked area and (c) amplified SEM image inside the cavity obtained.

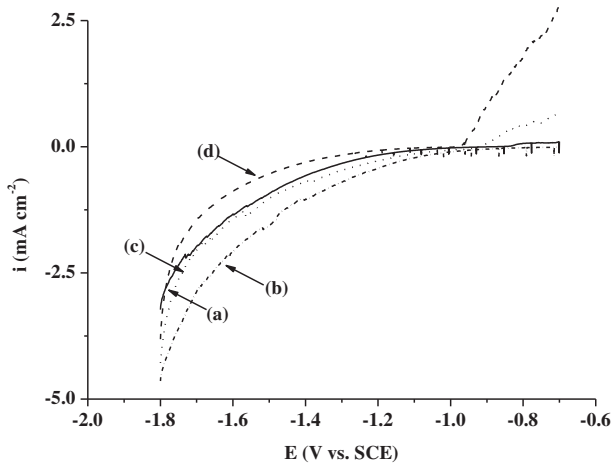


**Fig. 17.** Linear polarisation curve registered at 0.001 V s$^{-1}$ in a 0.5 M HAc, pH 3 solution for: (a) Al–4.0 wt%Zn, (b) Al–4.0 wt%Zn–0.5 wt.%Ga, (c) Al–4.0 wt.%Zn–2.5 wt.%Ga and (d) Al–4.0 wt.%Zn–5.0 wt.%Ga.

The polarisation measurements in acetic acid media confirm that the activation process of the Al ternary alloys was produced without the presence of an aggressive ion like chloride.

## 4. Discussion

According to the Pourbaix diagram of pure Ga, the theoretical value of the reversible potential of the $Ga/Ga_2O_3$ couple is −0.904 V(SCE) for a pH 3 [31]. Thus, this theoretical reversible potential ($E_{Ga/Ga_2O_3}$) is more negative than the corrosion potential ($E_{corr}$) of the Al–4.0 wt.%Zn–0.5 wt.%Ga alloy. Therefore, it would be possible that the Ga present in this alloy is oxidized. This does not occur for the Al–4.0 wt.%Zn–2.5 wt.%Ga and Al–4.0 wt.% Zn–5.0 wt.%Ga alloys, where the $E_{Ga/Ga_2O_3}$ value is more positive than the $E_{corr}$. Then, it is possible according to thermodynamic data the formation of $Ga_2O_3$ in the Al–4.0 wt.%Zn–0.5 wt.%Ga alloy which contributes to attain a more passive state with respect to the Al–4.0 wt.%Zn alloy (Fig. 3).

The experimental results also show that for the Al–4.0 wt.% Zn–*x* wt.%Ga alloy a concentration greater than 2.5 wt.% of Ga is required to reach an active state in chloride acid solution.

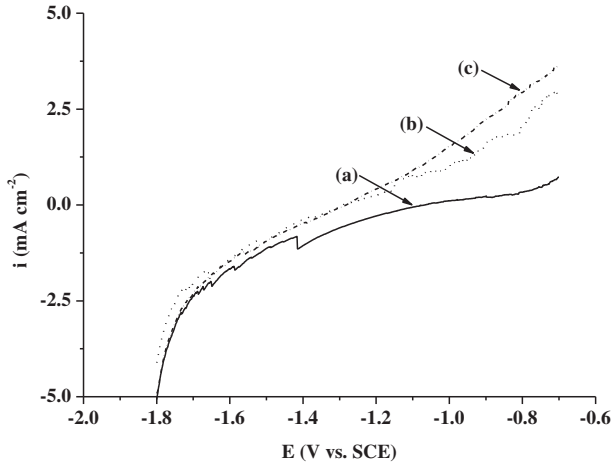


**Fig. 18.** Linear polarisation curve registered at 0.001 V s$^{-1}$ in a 0.5 M HAc, pH 3 solution for: (a) Al–0.2 wt.%In–0.5 wt.%Ga, (b) Al–0.2 wt.%In–2.5 wt.%Ga and (c) Al–0.2 wt.%In–5.0 wt.%Ga.

It was reported that the presence of Zn in the Al–Zn–Ga alloys resulted in higher efficiencies due to the better metallurgical homogeneity distribution of alloyed component [10]. The homogeneous distribution of attacked areas over the Al–4.0 wt.%Zn–5.0 wt.%Ga alloy surface (Fig. 4a and Fig. 8b) and can be explained considering its microstructure (small crystals with high Ga content (Fig. 1)).

The OCP measured in HAc solution was more positive than in chloride acid media due to the formation of a more passive film as a result of reaction between oxidised Al and acetate ion, according to the previous results obtained for an Al surface with Ga mechanically attached [29] and Al–Zn alloy with deposited In [30].

With respect to Al–In–Ga ternary alloys, no matter the amount of Ga used in the nominal composition (between 0.5 and 5.0 wt.%), the presence of a minimum quantity of In (0.2 wt.%) produces an active state in both chloride and acetic acid media. The OCP measured for the Al–0.2 wt.%In–5.0 wt.%Ga alloy was −1.76 and −1.50 V(SCE) in chloride and HAc solution, respectively. The displacement of OCP towards very negative values was not found by other authors who also investigated the electrochemical behaviour of Al–In–Ga alloys [32]. The discrepancy could be explained by considering the difference in the casting techniques used which determines the alloying elements distribution. The quenching of the melted sample in water at room temperature as was done in this work resulted in a homogenous distribution of alloying components. A partial segregation of active metals (In and Ga) at the grain boundaries is expected for the Al–In–Ga alloy obtained after cooling in air as was reported in Ref. [32].

Until now, the most active potentials in aqueous media were measured for Al-Hg alloys or for Al in solutions containing $Hg_2^{2+}$ ions (−1.60 V(SCE)) [7,33]. Our results demonstrate that small percentages of In in Al–In–Ga alloys significantly shift the OCP value. Likewise, the measured activation potentials coincide with those previously reported for Ga–1.0 wt.%Al amalgam and Ga-wetted Al electrodes immersed in chloride and HAc solutions [26], although for the latter systems the very reactive interface is not maintained for longer times. It has been postulated that the activation effect exerted by Ga on Al is due to the formation of a Ga–Al amalgam which detaches the Al oxide. The process is favoured by the exothermic Al ion hydrolysis reaction. It therefore appears that for the Al–In–Ga alloys the formation of a Ga–Al amalgam is also responsible for the activation process. It has been suggested that amalgam saturation due to Ga losses and the build-up of Al oxide contribute to the loss of activity.

The effects of heat treatment on activation of Al by In have been recently analysed [34]. It was considered that the activation of Al in chloride solution is a result of segregation of In in the alloy surface and that In particles may form an amalgam with Al. On the other hand, a very negative potential was measured for the Al–5.0 wt.% Zn alloy in an aerated 3.5% NaCl electrolyte containing $In^{3+}$ ions [35]. It was suggested that the incorporation of $In^+$ or $In^{2+}$ intermediates into the passive film leads to an increase in anionic vacancies and a decrease in the number of electrons, promoting active Al dissolution. Thus, for the activation of Al–In–Ga alloys it is possible that segregated In contributes to oxide destabilisation because it forms an amalgam with Al [29,34] and also because it modifies the oxide film properties. A smoother attack and more generalised corrosion were observed in all the cases studies in this paper by comparing with the pitting morphology obtained for pure Al in chloride solution. This kind of attacked morphology supports the theory of Ga–Al amalgam formation. The chill microstructure revealed for both alloys explains the homogeneous distribution of the attacked areas. Moreover, the amalgam activation mechanism is produced in both ternary Al alloys in acetic acid media without presence of aggressive anion like chloride, although at more positive corrosion potential.

## 5. Conclusions

Very negative potential were measured for Al–4.0 wt.% Zn–$x$ wt.%Ga ($x > 2.5$) and Al–0.2 wt.%In–$y$ wt.%Ga ($y > 0.5$) alloys in chloride and acetic acid media. The improvement of this active state is due to the oxidation of oxide free aluminium at the amalgam/electrolyte interface. The amalgam activation mechanism of the ternary alloys investigated takes place at potentials where adsorption of chloride is not feasible. The homogeneously distributed gallium in the alloys ensures the formation of the Ga–Al amalgam. The attacked areas are uniformly distributed on the electrode surface in ternary alloys, although smoother attack was observed for the case of Al-In-Ga alloys.

Al–0.2 wt.%In–$x$ wt.%Ga alloys have a more negative corrosion potential ($E_{corr}$) and a higher corrosion current density ($i_{corr}$) values compared to Al–4.0 wt.%Zn–$y$wt.%Ga alloys, for the same Ga composition. We consider that the Al–In–Ga alloy is a promising candidate alloy for further developments of sacrificial anodes.

## Acknowledgements

The financial support of the Secretaría de Ciencia y Técnica – UNS (PGI 24/M111/07), the Consejo Nacional de Investigaciones Científicas y Técnicas (CONICET-PIP 112-200801-0) and the Agencia Nacional de Promoción Científica y Tecnológica (ANPCYT PICT-2007-02308) is gratefully acknowledged. Dr. Luis A. Fabietti (Facultad de Matemática, Astronomía y Física, Universidad Nacional de Córdoba, Argentina) is acknowledged for obtaining the alloys.

## References

[1] W.M. Latimer, The Oxidation States of Elements and their Potentials in Aqueous Solutions, Prentice Hall, Englewood Cliffs, NJ, 1952.
[2] B.M. Ponchel, R.L. Horst, Mater. Protection 7 (1968) 38–41.
[3] J.F. Equey, S. Müller, J. Desilvestro, O. Haas, J. Electrochem. Soc. 139 (1992) 1499–1502.
[4] E. Budevski, I. IIiev, A. Kaisheva, A. Despić, K. Krsmanović, J. Appl. Electrochem. 19 (1989) 323–330.
[5] S. Müller, F. Holzer, J. Desilvestro, O. Haas, J. Appl. Electrochem. 26 (1996) 1217–1223.
[6] L. Legrand, A. Tranchant, R. Messino, Electrochim. Acta 39 (1994) 1427–1431.
[7] J.T. Reading, J.J. Newport, Mater. Protection 5 (1966) 15–18.
[8] S.B. Saidman, S.G. García, J.B. Bessone, J. Appl. Electrochem. 25 (1995) 252–258.
[9] C.B. Breslin, W.M. Carroll, Corros. Sci. 34 (1993) 1099–1109.
[10] E. Aragon, L. Cazenave-Vergez, E. Lanza, A. Giroud, A. Sebaoun, Br. Corros. J. 32 (1997) 263–268.
[11] C.D.S. Tuck, J.A. Hunter, G.M. Scamans, J. Electrochem. Soc. 134 (1987) 2970–2981.
[12] A. Mance, D. Cerović, A. Mihajlović, J. Appl. Electrochem. 15 (1985) 415–420.
[13] C.B. Breslin, W.M. Carroll, Corros. Sci. 33 (1992) 1735–1746.
[14] H.A. El Shayeb, F.M. Abd El Wahab, S. Zein El Abedin, Corros. Sci. 43 (2001) 643–654.
[15] A.R. Despić, R.M. Stevanović, A.M. Vorkapiće, A new method of obtaining electrochemically active aluminium, in: 35th ISE Meeting, Paper A2-19, Extended Abstracts, Berkeley, CA (1984).
[16] L. Bai, B.E. Conway, J. Appl. Electrochem. 22 (1992) 131–139.
[17] I.L. Müller, J.R. Galvele, Corros. Sci. 17 (1977) 995–1007.
[18] M.C. Reboul, M.C. Dellale, Mater. Performance 19 (1980) 35–40.
[19] H.A. El Shayeb, F.M. Abd El Wahab, S. Zein El Abedin, Corros. Sci. 43 (2001) 655–669.
[20] J.C. Lin, H.C. Shih, J. Electrochem. Soc. 134 (1987) 817–823.
[21] S.L. Wolfson, Mater. Performance 33 (1994) 22–28.
[22] A.G. Muñoz, S.B. Saidman, J.B. Bessone, Corros. Sci. 44 (2002) 2171–2182.
[23] C.B. Breslin, L.P. Friery, W.M. Carroll, Corros. Sci. 36 (1994) 85–97.
[24] D.O. Flamini, S.B. Saidman, J.B. Bessone, Thin Sol. Films 515 (2007) 7880–7885.
[25] D.O. Flamini, S.B. Saidman, J. Appl. Electrochem. 38 (2008) 663–668.
[26] D.O. Flamini, L. Cunci, S.B. Saidman, Mater. Chem. Phys. 108 (2008) 33–38.
[27] A.R. El-Sayed, A.M. Shaker, H.M. Abd El-Lateef, Corros. Sci. 52 (2010) 72–81.
[28] A.N. Frumkin, N.B. Grigoryev, I.A. Bagotskaya, Dolk. Akad. Nauk. SSSR 157 (1964) 957–962.
[29] D.O. Flamini, S.B. Saidman, J.B. Bessone, Corros. Sci. 48 (2006) 1413–1425.
[30] J.B. Bessone, D.O. Flamini, S.B. Saidman, Corros. Sci. 47 (2005) 95–105.
[31] M. Pourbaix, Atlas of the Electochemical Equilibria in Aqueous Solution, Pergamon Press, 1966.
[32] S. Zeim El Abedim, F. Endres, J. Appl. Electrochem. 34 (2004) 1071–1080.
[33] J.B. Bessone, Corr. Sci. 48 (2006) 4243–4256.
[34] B. Graver, A.T.J. Van Helvoort, K. Nisancioglu, Corros. Sci. 52 (2010) 3774–3781.
[35] A. Venugopal, V.S. Raja, Corros. Sci. 39 (1997) 2053–2065.